VIETNAM ACADEMY OF SCIENCE AND TECHNOLOGY

Vietnam Journal of MECHANICS

Volume 35 Number 1

ISSN 0866-7136

VN INDEX 12.666

1
2013
35th Anniversary

Vietnam Journal of Mechanics, VAST, Vol. 35, No. 1 (2013), pp. 79 – 91

ISOGEOMETRIC ANALYSIS OF TWO–DIMENSIONAL PIEZOELECTRIC STRUCTURES

Hoang H. Truong[1], **Chien H. Thai**[2], **H. Nguyen-Xuan**[2,3]
[1] *University of Technical Education of Ho Chi Minh City, Vietnam*
[2] *Ton Duc Thang University, Ho Chi Minh City, Vietnam*
[3] *University of Science Ho Chi Minh City, VNU-HCM, Vietnam*

Abstract. The isogeometric analysis (IGA) that integrates Computer Aided Design (CAD) and Computer Aided Engineering (CAE) is found so far the effectively numerical tool for the analysis of a variety of practical problems. In this paper, we develop further the NURBS based isogeometric analysis framework for piezoelectric structures. The method employs the NURBS basis functions in both geometry representation and analysis. The main advantages of the present method are capable of handling the exact geometry of conic sections and making the flexibility of refinement and degree elevation with an arbitrary continuity of basic functions. These features results in high accuracy of approximate solutions for practical applications, especially piezoelectric problems. Three numerical examples are provided to validate excellent performance of the present method.

Keywords: NURBS, isogeometric analysis, piezoelectric materials, smart materials.

1. INTRODUCTION

In recent years, the use of smart materials has become widespread and almost commonplace. The technology employed in piezoelectric applications in particular, has reached a mature level, and piezoelectric materials are frequently used in engineering applications. Piezoelectric materials transfer electric energy to mechanical energy and vice versa, and can therefore be used as either actuators or sensors, or both. Applications include ultrasonic transducers for sonar and medical purposes, compact piezoelectric motors, structural monitoring or active damping elements, and even ignition systems [1,2]. Analytical solutions which are, however, very useful as benchmark problems to problems involving piezoelectric materials are often difficult to find unless some geometries and boundary conditions are relatively simple. Numerical methods have been devised to find the approximate solution of these piezoelectric problems. Among them, the finite element method has become a standard modelling utility for various physical processes, including piezoelectricity.

In development of advanced computational methodologies, Hughes *et al.* [3] have recently proposed a NURBS-based isogeometric analysis to bridge the gap between Computer Aided Design (CAD) and Finite Element Analysis (FEA). In contrast to the standard FEM with Lagrange polynomial basis, isogeometric approach utilized more general basis

functions such as Non-Uniform Rational B-splines (NURBS) that are common in CAD approaches. Isogeometric analysis is thus very promising because it can directly use CAD data to describe both exact geometry and approximate solution. For structural mechanics, isogeometric analysis has been extensively studied for nearly incompressible linear and non-linear elasticity and plasticity problem [4], structural vibrations [5], the composite Reissner-Mindlin plates [6], the Reissner-Mindlin shells [7], Kirchhoff-Love shells [8-10], the large deformation with rotation-free [11] and structural shape optimization [12], etc. In this paper, a NURBS-based isogeometric analysis formulation is presented for piezoelectric material structures. The isogeometric stiffness matrices are constructed for quadratic, cubic and quartic elements. Several numerical examples are illustrated to demonstrate the effectiveness of the present method.

The paper is arranged as follows: a brief of the B-spline and NURBS surface is described in section 2. Section 3 describes an isogeometric approximation for piezoelectric materials. The numerical examples are illustrated in section 4. Finally, we close our paper with some concluding remarks.

2. NURBS-BASED ISOGEOMETRIC ANALYSIS FUNDAMENTALS

2.1. Knot Vectors and Basis Functions

In one-dimensional problems, a knot vector $\boldsymbol{\Xi}$ is the set of coordinates in the parametric space as

$$\boldsymbol{\Xi} = \{\xi_1, \xi_2, \ldots, \xi_{n+p+1}\} \tag{1}$$

where p, n are the order of the B-Spline and the number of basis functions associated with control points, respectively. The interval $\begin{bmatrix}\xi_1 & \xi_{n+p+1}\end{bmatrix}$ is called a patch. Given a knot vector, the B-spline basis functions $N_{i,p}(\xi)$ of order $p = 0$ are defined recursively on the corresponding knot vector as follows

$$N_{i,0}(\xi) = \begin{cases} 1 & \text{if } \xi_i < \xi < \xi_{i+1} \\ 0 & \text{otherwise} \end{cases} \tag{2}$$

The basis functions of $p > 1$ are defined by the following recursion formula

$$N_{i,p}(\xi) = \frac{\xi - \xi_i}{\xi_{i+p} - \xi_i} N_{i,p-1}(\xi) + \frac{\xi_{i+p+1} - \xi}{\xi_{i+p+1} - \xi_{i+1}} N_{i+1,p-1}(\xi) \quad \text{with } p > 1 \tag{3}$$

2.2. NURBS Surface

The B-spline curve is defined as

$$\mathbf{C}(\xi) = \sum_{i=1}^{n} N_{i,p}(\xi)\, \mathbf{P}_i \tag{4}$$

where $\mathbf{P}_i$ are the control points and $N_{i,p}(\xi)$ is the p^{th}-degree B-spline basis function defined on the open knot vector. Fig. 1 illustrates a set of cubic B-splines curves and cubic B-spline basis functions for open uniform knot vectors $\boldsymbol{\Xi} = \{0, 0, 0, 0, 1/4, 1/2, 3/4, 1, 1, 1, 1\}$.

The B-spline surfaces are defined by the tensor product of basis functions in two parametric dimensions ξ and η with two knot vectors $\boldsymbol{\Xi} = \{\xi_1, \xi_2, ..., \xi_{n+p+1}\}$ and $H =$

$\{\eta_1, \eta_2, ..., \eta_{m+q+1}\}$ are expressed as follows

$$\mathbf{S}(\xi, \eta) = \sum_{i=1}^{p} \sum_{j=1}^{q} N_{i,p}(\xi) M_{j,q}(\eta) \mathbf{P}_{i,j} \tag{5}$$

where $P_{i,j}$ is the bidirectional control net, $N_{i,p}(\xi)$ and $M_{j,q}(\eta)$ are the B-spline basis functions defined on the knot vectors over an $n \times m$ net of control points $\mathbf{P}_{i,j}$. To have

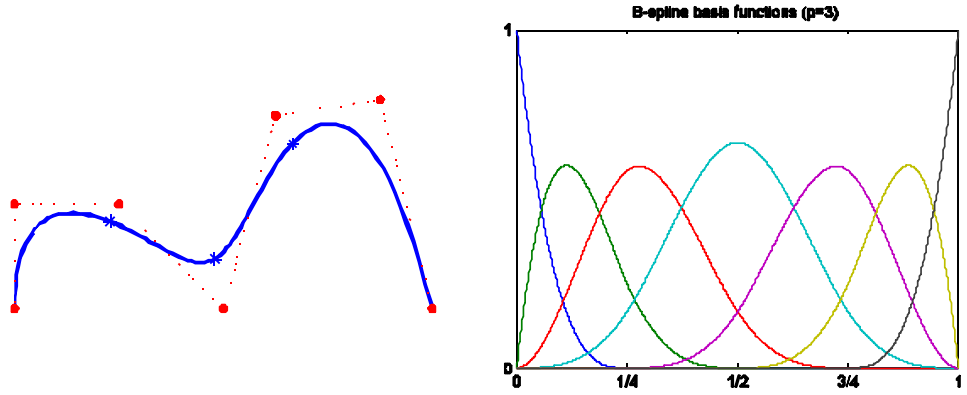

(a) (b)

Fig. 1. An illustration of cubic B-splines curves: a) Cubic B-spline curves; b) basis functions

the same notation as the finite element method, we identify the logical coordinates (i, j) of the B-spline surface with the traditional notation of a node A. Eq. (5) is now rewritten as

$$\mathbf{S}(\xi, \eta) = \sum_{A}^{nm} N_A(\xi, \eta) \mathbf{P}_A \tag{6}$$

where $N_A(\xi, \eta) = N_{i,p}(\xi) M_{j,q}(\eta)$ is the shape function associated with node A. Similar to B-Splines, a NURBS surface is defined as

$$\mathbf{S}(\xi, \eta) = \sum_{A=1}^{nm} R_A(\xi, \eta) \mathbf{P}_A \tag{7}$$

where $R_A = \dfrac{N_A w_A}{\sum\limits_{A}^{nm} N_A w_A}$ and w_A are the rational basis functions and the weight functions, respectively.

3. AN ISOGEOMETRIC ANALYSIS FORMULATION OF 2D PIEZOELECTRIC PROBLEMS

The piezoelectric constitutive equations for a two-dimensional can be expressed under the form as [1]

$$\begin{bmatrix} T_x \\ T_z \\ T_{xz} \end{bmatrix} = \begin{bmatrix} c_{11} & c_{13} & 0 \\ c_{13} & c_{33} & 0 \\ 0 & 0 & c_{55} \end{bmatrix} \begin{bmatrix} S_x \\ S_z \\ S_{xz} \end{bmatrix} - \begin{bmatrix} 0 & e_{31} \\ 0 & e_{33} \\ e_{15} & 0 \end{bmatrix} \begin{bmatrix} E_x \\ E_z \end{bmatrix}$$
$$\begin{bmatrix} D_x \\ D_z \end{bmatrix} = \begin{bmatrix} 0 & 0 & e_{15} \\ e_{31} & e_{33} & 0 \end{bmatrix} \begin{bmatrix} S_x \\ S_z \\ S_{xz} \end{bmatrix} - \begin{bmatrix} \varepsilon_{11} & 0 \\ 0 & \varepsilon_{33} \end{bmatrix} \begin{bmatrix} E_x \\ E_z \end{bmatrix} \tag{8}$$

Eq. (8) also can be written matrix form as

$$\begin{aligned} \mathbf{T} &= \mathbf{c}^{\mathbf{E}}\mathbf{S} - \mathbf{e}^T\mathbf{E} \\ \mathbf{D} &= \mathbf{e}\mathbf{S} + \boldsymbol{\varepsilon}^{\mathbf{S}}\mathbf{E} \end{aligned} \tag{9}$$

where $\mathbf{T}$, $\mathbf{S}$, $\mathbf{E}$ and $\mathbf{D}$ are the stress vector, the strain vector, the electric field and the electric displacement, respectively. $\mathbf{c}^{\mathbf{E}}$ is the elastic coefficients at constant $\mathbf{E}$, $\boldsymbol{\varepsilon}^{\mathbf{S}}$ is the dielectric coefficients at constant $\mathbf{S}$ and $\mathbf{e}$ is the piezoelectric coupling coefficients.

The strain displacement and electric field potential relationships are expressed by

$$\mathbf{S} = \mathbf{L}\mathbf{u} \tag{10}$$

$$\mathbf{E} = -grad\phi \tag{11}$$

where $\mathbf{L}$ is the symmetric gradient operator defined such as

$$\mathbf{L} = \begin{bmatrix} \dfrac{\partial}{\partial x} & 0 & \dfrac{\partial}{\partial y} \\ 0 & \dfrac{\partial}{\partial y} & \dfrac{\partial}{\partial x} \end{bmatrix}^T \tag{12}$$

A weak form of the dynamic model for 2D piezoelectric can be briefly expressed as [1]

$$\int_\Omega \delta\mathbf{S}^T\mathbf{T}\mathrm{d}\Omega + \int_\Omega \delta\mathbf{u}^T\rho\ddot{\mathbf{u}}\mathrm{d}\Omega - \int_\Omega \delta\mathbf{E}^T\mathbf{D}\mathrm{d}\Omega - \int_\Omega \delta\mathbf{u}^T\bar{\mathbf{f}}\mathrm{d}\Omega - \int_\Gamma \delta\mathbf{u}^T\bar{\mathbf{t}}\mathrm{d}\Gamma + \int_\Gamma \delta\boldsymbol{\psi}^T\mathbf{q}_s d\Gamma = 0 \tag{13}$$

Using the NURBS basis functions, the variables are the displacement and the electric potential at all control points, which can be expressed as

$$\mathbf{u} = \sum_{A=1}^{nm} \begin{bmatrix} R_A & 0 \\ 0 & R_A \end{bmatrix} \begin{Bmatrix} u_A \\ v_A \end{Bmatrix} = \sum_{A=1}^{nm} \mathbf{R}_A\mathbf{q}_A \quad \text{and} \quad \boldsymbol{\phi} = \sum_{A=1}^{nm} R_A\phi_A \tag{14}$$

where $n \times m$ is the number basis functions. R_A, $\mathbf{q}_A = \begin{bmatrix} u_A & v_A \end{bmatrix}^T$ and ϕ_A are rational basic functions, the degrees of freedom of $\mathbf{u}$ and the degrees of freedom of $\boldsymbol{\Phi}$ associated with a control point A, respectively.

Substituting the approximations Eq. (14) into equations Eqs. (10) and (11), we obtain

$$\mathbf{S} = \sum_{A=1}^{nm} \mathbf{B}_A^u \mathbf{q}_A \quad \text{and} \quad \mathbf{E} = \sum_{A=1}^{nm} \mathbf{B}_A^\phi \phi_A \tag{15}$$

where

$$\mathbf{B}_A^u = \begin{bmatrix} R_{A,x} & 0 \\ 0 & R_{A,y} \\ R_{A,y} & R_{A,x} \end{bmatrix} \quad \text{and} \quad \mathbf{B}_A^\phi = \begin{bmatrix} R_{A,x} \\ R_{A,y} \end{bmatrix} \tag{16}$$

Substituting Eqs. (15) and (16) into (13), we have a set of piezoelectric static equations

$$\mathbf{M}_{uu}\ddot{\mathbf{u}} + \mathbf{K}_{uu}\mathbf{u} + \mathbf{K}_{u\phi}\mathbf{\Phi} = \mathbf{f} \tag{17}$$

$$\mathbf{K}_{\phi u}\mathbf{u} + \mathbf{K}_{\phi\phi}\mathbf{\Phi} = \mathbf{g} \tag{18}$$

or in matrix form

$$\begin{bmatrix} \mathbf{M}_{uu} & 0 \\ 0 & 0 \end{bmatrix} \begin{bmatrix} \ddot{\mathbf{u}} \\ \ddot{\mathbf{\Phi}} \end{bmatrix} + \begin{bmatrix} \mathbf{K}_{uu} & \mathbf{K}_{u\phi} \\ \mathbf{K}_{\phi u} & \mathbf{K}_{\phi\phi} \end{bmatrix} \begin{bmatrix} \mathbf{u} \\ \mathbf{\Phi} \end{bmatrix} = \begin{bmatrix} \mathbf{f} \\ \mathbf{g} \end{bmatrix} \tag{19}$$

where

$$\begin{gathered} \mathbf{M}_{uu} = \int_\Omega \rho \mathbf{R}_A^T \mathbf{R}_A \,\mathrm{d}\Omega;\ \mathbf{K}_{uu} = \int_\Omega \mathbf{B}_A^{uT} \mathbf{c}^E \mathbf{B}_A^u \,\mathrm{d}\Omega; \\ \mathbf{K}_{u\phi} = \int_\Omega \mathbf{B}_A^{\phi T} \mathbf{e}^T \mathbf{B}_A^\phi \,\mathrm{d}\Omega;\ \mathbf{K}_{\phi\phi} = -\int_\Omega \mathbf{B}_A^{\phi T} \boldsymbol{\varepsilon}^S \mathbf{B}_A^\phi \,\mathrm{d}\Omega;\ \mathbf{K}_{\phi u} = \mathbf{K}_{u\phi}^T; \\ \mathbf{f} = \int_\Omega \mathbf{R}_A^T \bar{\mathbf{f}} \,\mathrm{d}\Omega + \int_\Gamma \mathbf{R}_A^T \bar{\mathbf{t}} \,\mathrm{d}\Gamma \text{ and } \mathbf{g} = \int_\Gamma \mathbf{R}_A^T \mathbf{q}_s \,\mathrm{d}\Gamma. \end{gathered} \tag{20}$$

4. NUMERICAL RESULTS

4.1. Infinite piezoelectric plate with a circular hole

Consider a piezoelectric plate with a central circular cavity subjected to a uniform uniaxial far-field stress $\sigma_\infty = 10$ in the y direction as shown in Fig. 2. This example is used to show the efficiency of the developed elements in predicting stresses in a stress concentration problem. The reference solution can be found in [2]. In this example we

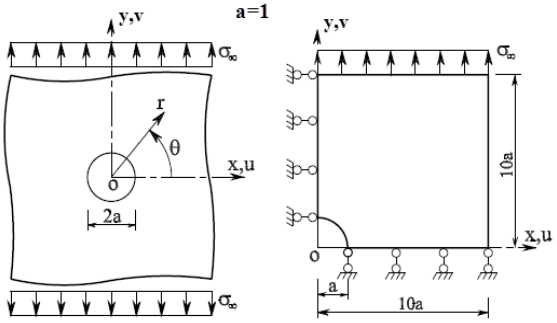

Fig. 2. An infinite piezo-plate with a circular hole subjected to the far-field stress

used the PZT-4 material with its properties are given in Tab. 1.

Table 1. The PZT-4 material

$c_{11} = 12.6e4$ N/mm^2	$e_{15} = 12.7e6$ pC/mm^2
$c_{13} = 7.43e4$ N/mm^2	$e_{31} = -5.2e6$ pC/mm^2
$c_{12} = 7.78e4$ N/mm^2	$e_{33} = 15.1e6$ pC/mm^2
$c_{33} = 11.5e4$ N/mm^2	$\varepsilon_{11} = 6.464e9$ pC/GVmm
$c_{55} = 2.56e4$ N/mm^2	$\varepsilon_{33} = 5.622e9$ pC/GVmm

Table 2. Control net for the plate with a circular hole

i	$P_{i,1}$	$P_{i,2}$	$P_{i,3}$	$P_{i,4}$
1	(0, 1)	(0, 3.4278)	(0, 7.75)	(0, 10)
2	(0.4142, 1)	(0.5954, 3.4278)	(5.375, 7.75)	(10, 10)
3	(1, 0.4142)	(3.4278, 0.5954)	(7.75, 5.3750)	(10, 10)
4	(1, 0)	(3.4278, 0)	(7.75, 0)	(10, 0)

Table 3. Weights for the plate with a circular hole

i	$P_{i,1}$	$P_{i,2}$	$P_{i,3}$	$P_{i,4}$
1	1	1	1	1
2	0.8536	1	1	1
3	0.8536	1	1	1
4	1	1	1	1

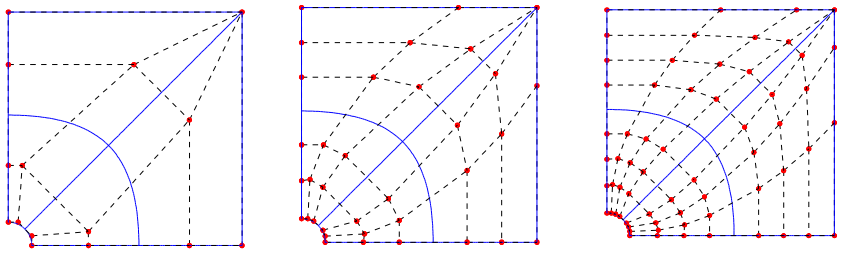

(a) (b) (c)

Fig. 3. Coarse mesh and control net for the infinite piezo-plate with a circular hole: a) quadratic; b) cubic and c) quartic elements.

Due to its symmetry, one fourth of the plate is modeled. A circular hole is represented the exact by a rational quadratic basis. The coarsest mesh, $\mathbf{E}\times\mathbf{H}$, is defined by the knot vectors $\mathbf{E} = \{0\ 0\ 0\ 0.5\ 1\ 1\ 1\}$ and $\mathbf{H} = \{0\ 0\ 0\ 0.5\ 1\ 1\ 1\}$. The exact geometry is represented with only four elements based on 16 control points, as shown in Fig. 3. The geometric data are given in Tabs. 2 and 3. Fig. 4 illustrates the first three meshes of an infinite piezo-plate.

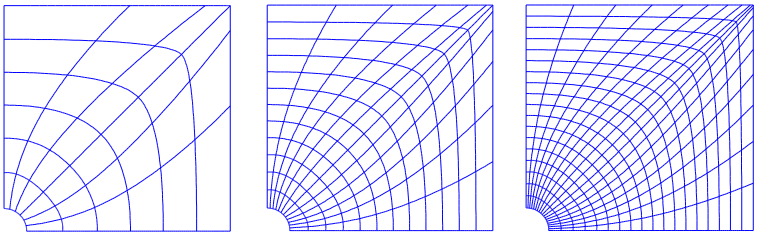

Fig. 4. NURBS meshes produced by h-refinement (knot insertion)

The results obtained from NURBS are compared with the reference solution by Y. Weian and H. Wang [2]. Fig. 5 shows the distribution of σ_r and σ_θ along the line $\theta = 0$ (x axis

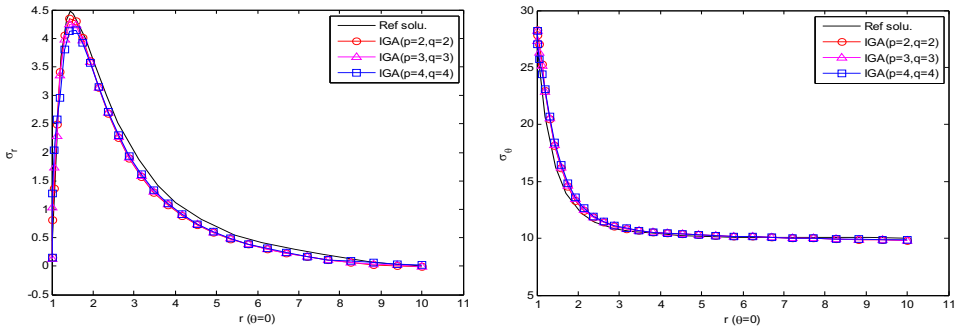

Fig. 5. Distribution of σ_r and σ_θ along the line $\theta = 0$

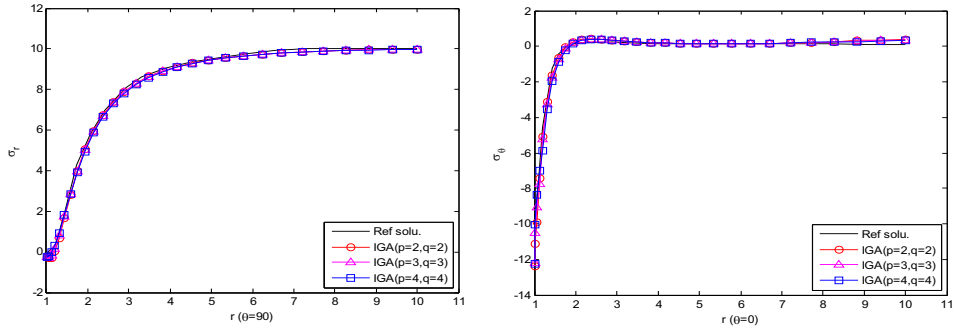

Fig. 6. Distribution of σ_r and σ_θ along the line $\theta = \pi/2$

in Fig. 2). It can be seen from Fig. 5 that σ_θ reaches maximum value at the intersection of the hole and the x axis. Fig. 6 describes the distribution of σ_r and σ_θ along the line $\theta = \pi/2$ (y axis in Fig. 2). The minimum value of σ_θ is obtained at the position where the hole intersects the y axis. The obtained result from present method matches well with the reference solution [2].

4.2. Single-layer piezoelectric strip in shear deformation

Next we consider the shear deformation of a 1×1 mm single-layer square strip polarized in the y direction. The strip is subjected to a combined loading of pressure σ_0 in the y direction and an applied voltage V_0 as depicted on Fig. 7. The material PZT-5 is

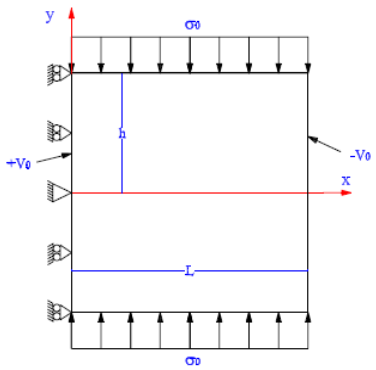

Fig. 7. The PZT-5 material

Table 4. Weights for the plate with a circular hole

$s_{11} = 16.4e-4$ mm^2/N	$d_{31} = -172e-9$ mm/V
$s_{13} = -7.22e-6$ mm^2/N	$d_{33} = 374e-9$ mm/V
$s_{33} = 18.8e-6$ mm^2/N	$d_{15} = 584e-9$ mm/V
$s_{55} = 47.5e-6$ mm^2/N	$L = 1$ mm; $h = 0.5$ mm
$g_{11} = 1.53105e-8$ N/V^2	$\sigma_0 = -5$ N/mm^2; $V_0 = 1e-6$ V
$g_{33} = 1.505e-8$ N/V^2	

used and its properties are summarized in Tab. 4. For this problem, the elastic coefficients, the dielectric coefficients and the piezoelectric coupling coefficients are unavailable and then they can be calculated as [1]

$$\mathbf{c}^{\mathbf{E}} = \begin{bmatrix} s_{11} & s_{13} & 0 \\ s_{13} & s_{33} & 0 \\ 0 & 0 & s_{55} \end{bmatrix}^{-1}, \ \mathbf{e}^T = \mathbf{c}^{\mathbf{E}}\mathbf{d}^T \text{ and } \boldsymbol{\varepsilon}^{\mathbf{S}} = \boldsymbol{\varepsilon}^{\mathbf{T}} - \mathbf{d}\mathbf{c}^{\mathbf{E}}\mathbf{d}^T \tag{21}$$

where

$$\boldsymbol{\varepsilon}^{\mathbf{T}} = \begin{bmatrix} g_{11} & 0 \\ 0 & g_{22} \end{bmatrix} \text{ and } \mathbf{d} = \begin{bmatrix} d_{11} & d_{13} & d_{15} \\ d_{31} & d_{33} & 0 \end{bmatrix} \tag{22}$$

Mechanical boundary conditions are applied to the upper and lower sides of the strip:

$$T_{yy}(x, y = \pm h) = \sigma_0, \quad T_{xy}(x = L, y) = 0, \quad T_{xy}(x, y = \pm h) = 0,$$
$$T_{xx}(x = L, y) = 0, \qquad u(x = 0, y) = 0, \qquad v(x = 0, y = 0) = 0,$$

and electrical boundary conditions is applied to the left and right sides of the strip :

$$\varphi(x = 0, y) = +V_0, \quad \varphi(x = L, y) = -V_0, \quad \varphi_y(x, y = \pm h) = 0,$$

The analytical solution for this problem is given in Ohs *et al.* [1]

$$u = s_{13}\sigma_0 x; \quad v = \frac{d_{15}V_0 x}{h} + s_{33}\sigma_0 y \quad \text{and} \quad \phi = V_0\left(1 - 2\frac{x}{L}\right)$$

The horizontal displacement and vertical displacement at the central line ($y = 0$) of the single-layer piezoelectric strip are shown in Fig. 8. The results are compared with the analytical solution in Ohs *et al.* [1]. It can be observed that the results of the present method are in excellent agreement with the analytical solutions. Fig. 9 shows the electric potential at the central line ($y = 0$) of the single-layer piezoelectric strip. Again, the obtained results match well with the analytical solutions given in [1].

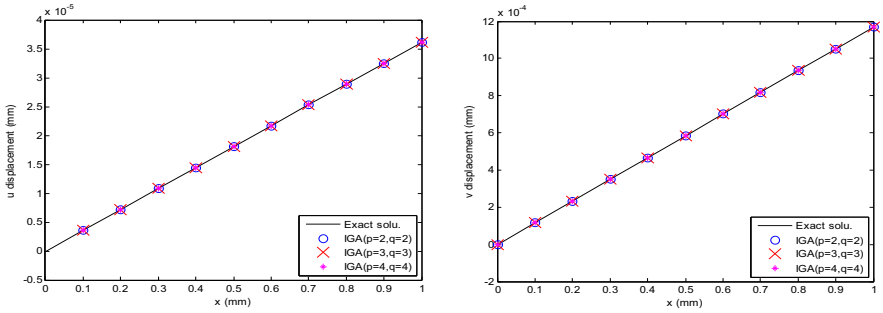

Fig. 8. Variation of horizontal displacement u and vertical displacement v at the central line ($y = 0$) of the single-layer piezoelectric strip in IGA quadratic, cubic and quartic elements

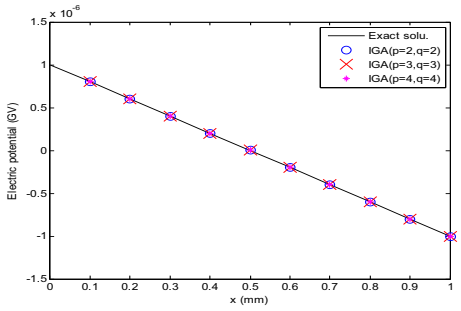

Fig. 9. Variation of electric potential ϕ at the central line ($y = 0$) of the single-layer piezoelectric strip in IGA quadratic, cubic and quartic elements

4.3. An extension to free vibration problem

This example is an eigenvalue analysis of a piezoelectric transducer consisting of a piezoelectric wall made of PZT4 material with brass end caps as shown in Fig. 10. The piezoelectric material is electroded on both the inner and outer surfaces. This problem has been investigated numerically by Liu *et al.* (2003) [13] and experimentally by Mercer *et al.* (1987) [14]. It is also a typical example described in Section 5.1.1 of ABAQUS Example Problems Manual [15]. The transducer is modeled as an axisymmetric problem.

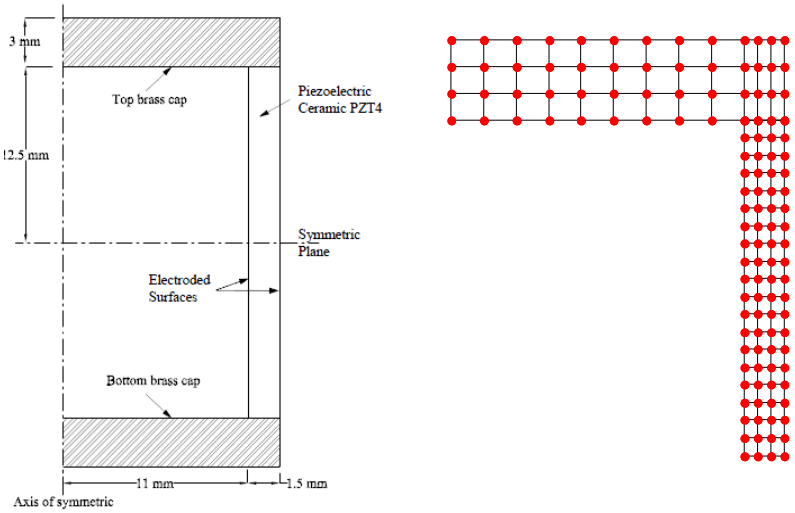

Fig. 10. Representative sketch and domain discretization control net of a piezoelectric transducer

The material properties of PZT4 are as

$$\rho = 7500 \text{ kgm}^{-3}$$

$$c = \begin{bmatrix} 115.4 & 74.28 & 74.28 & 0 & 0 & 0 \\ 74.28 & 139.0 & 77.84 & 0 & 0 & 0 \\ 74.28 & 77.84 & 139.0 & 0 & 0 & 0 \\ 0 & 0 & 0 & 25.64 & 0 & 0 \\ 0 & 0 & 0 & 0 & 25.64 & 0 \\ 0 & 0 & 0 & 0 & 0 & 25.64 \end{bmatrix} \text{ GPa}$$

$$e = \begin{bmatrix} 15.08 & -5.207 & -5.207 & 0 & 0 & 0 \\ 0 & 0 & 0 & 12.71 & 0 & 0 \\ 0 & 0 & 0 & 0 & 12.74 & 0 \end{bmatrix} \text{ Cm}^{-2}$$

$$g = \begin{bmatrix} 5.872 & 0 & 0 \\ 0 & 6.752 & 0 \\ 0 & 0 & 6.752 \end{bmatrix} \times 10^{-9} \text{ Fm}^{-1}$$

And the material properties of brass are

$$\rho = 8500 \text{ kgm}^{-3}; \quad E = 10.4 \times 10^{10} \text{ Pa}; \quad v = 0.37$$

To illustrate we evaluate the performance of the present method using only the quadratic NURBS element. Tab. 5 shows the first five frequencies, and the relative error percentages compared with experimental results are given in parentheses. Fig. 11 depicts five modes given in Table using the quadratic NURBS element. It is again seen that the present method outperforms with other published approaches.

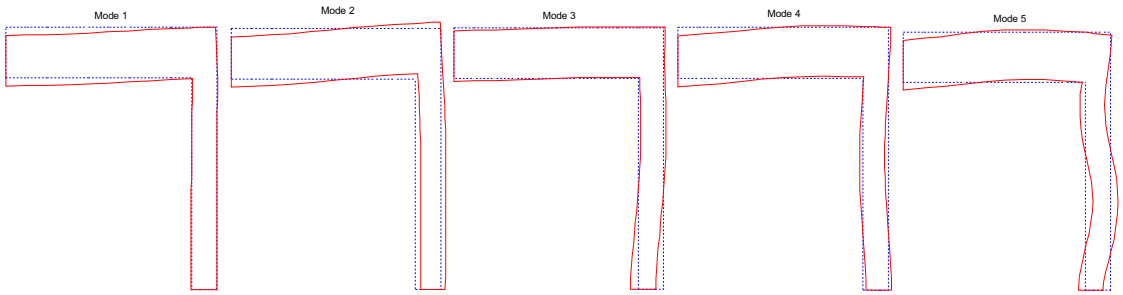

Fig. 11. Eigenmodes for the piezoelectric transducer

Table 5. Eigenvalues (kHz) of the piezoelectric transducer

Element type	Mode 1	Mode 2	Mode 3	Mode 4	Mode 5
T3 (272 elements)	19.98 (7.42%)	43.31 (22.34%)	62.78 (15.83%)	67.78 (7.08%)	94.23 (6.12%)
Q4 (136 elements)	19.7 (5.91%)	42.9 (21.19%)	61.1 (12.73%)	66.7 (5.37%)	92.2 (3.83%)
IGA (58 elements)	18.73 (0.69%)	39.45 (11.4%)	61.44 (13.3%)	67.82 (7.14%)	87.69 (–1.25%)
CAX4E (320 elements)	18.6	40.3	57.8	64.2	88.1
CAX8RE (80 elements)	18.6	40.3	57.6	64.2	87.6
Experimental	18.6	35.4	54.2	63.3	88.8

where CAX4E and CAX8RE are ABAQUS 4-node axisymmetric elements and 8-node axisymmetric elements respectively [15].

5. CONCLUSIONS

The isogeometric analysis formulation has been developed for 2D-piezoelectric structures. The quadratic, cubic and quartic elements are utilized and their results are well compared with those of several existing methods. Main advantages of the present method are to maintain the exact geometry of problems containing conic sections and to provide a flexible way to make refinement, and degree elevation. It allows us to easily achieve the smoothness with arbitrary continuity order compared with the traditional FEM. The method is thus very useful to apply for analyzing piezoelectric structures.

ACKNOWLEDGEMENT

This research is funded by Vietnam National University Ho Chi Minh City (VNU-HCM).

REFERENCES

[1] R. R. Ohs and N. R. Aluru, Meshless analysis of piezoelectric devices, *Computational Mechanics*, **27**, (2001), 23-36.

[2] Y. Weian and H. Wang, Virtual boundary element integral method for 2-D piezoelectric media, *Finite Elements in Analysis and Design*, **41**, (2005), 875–891.

[3] T. J. R. Hughes, J. A. Cottrell, and Y. Bazilevs, Isogeometric analysis: CAD, finite elements, NURBS, exact geometry and mesh refinement, *Computer Methods in Applied Mechanics and Engineering*, **194**, (2005), 4135–4195.

[4] T. Elguedj, Y. Bazilevs, V. Calo, T. Hughes, B and F projection methods for nearly incompressible linear and non-linear elasticity and plasticity using higher-order nurbs elements, *Computer Methods in Applied Mechanics and Engineering*, **197**, (2008), 2732–2762.

[5] J. A. Cottrell, A. Reali, Y. Bazilevs, and T. J. R. Hughes, Isogeometric analysis of structural vibrations, *Computer Methods in Applied Mechanics and Engineering*, **195**, (2006), 5257–5296.

[6] Chien H. Thai, H. Nguyen-Xuan, N. Nguyen-Thanh, Hien T. Le, T. Nguyen-Thoi and T. Rabczuk, Static, free vibration, and buckling analysis of laminated composite Mindlin-Ressner plates using NURBS-based isogeometric approach, *International Journal for Numerical Methods in Engineering*, 91, (2012), 571Q603.

[7] D. J. Benson, Y. Bazilevs, M. C. Hsu, T. J. R. Hughes, Isogeometric shell analysis: The Reissner–Mindlin shell, *Computer Methods in Applied Mechanics and Engineering*, **199**, (2010), 276–289.

[8] J. Kiendl, K. U. Bletzinger, J. Linhard, R. Wuchner, Isogeometric shell analysis with Kirchhoff-Love elements, *Computer Methods in Applied Mechanics and Engineering*, **198**, (2009), 3902–3914.

[9] N. Nguyen-Thanh, J. Kiendl, H. Nguyen-Xuan, R. Wüchner, K.U. Bletzinger, Y. Bazilevs, T. Rabczuk, Rotation free isogeometric thin shell analysis using PHT-splines, *Computer Methods in Applied Mechanics and Engineering*, **200**, (2011), 3410-3424.

[10] J. Kiendl, Y. Bazilevs, M. C. Hsu, R. Wchner, and K. U. Bletzinger, The bending strip method for isogeometric analysis of Kirchhoff-Love shell structures comprised of multiple patches, *Computer Methods in Applied Mechanics and Engineering*, **199**, (2010), 2403–2416.

[11] D. J. Benson, Y. Bazilevs, M. C. Hsu, and T.J.R. Hughes, A large deformation, rotation-free, isogeometric shell, *Computer Methods in Applied Mechanics and Engineering*, **200**, (2011), 1367–1378.

[12] W. A. Wall, M. A. Frenzel, and C. Cyron, Isogeometric structural shape optimization, *Computer Methods in Applied Mechanics and Engineering*, **197**, (2008), 2976–2988.
[13] G. R. Liu, K. Y. Dai, K. M. Lim and Y. T. Gu, A radial point interpolation method for simulation of two-dimensional piezoelectric structures, *Smart Mater. Struct. 12*, (2003), 171–180.
[14] Mercer C. D., Reddy B. D. and Eve R. A., Finite element method for piezoelectric media, *Applied Mechanics Research Unit Technical Report No 92 University of Cape Town/CSIR*, (1987).
[15] ABAQUS Example Problems Manual (2008).

Received January 02, 2012

VIETNAM ACADEMY OF SCIENCE AND TECHNOLOGY
VIETNAM JOURNAL OF MECHANICS VOLUME 35, N. 1, 2013

CONTENTS